Nanoscale

PAPER

View Article Online
View Journal | View Issue

Cite this: *Nanoscale*, 2025, **17**, 22958

Influence of nanoendoscopy AFM imaging of intracellular structures on cell proliferation and stress response

Mohammad Mubarak Hosain, [a] Mohammad Shahidul Alam, [a] Takehiko Ichikawa, [b] Keisuke Miyazawa, [b,c] Kazuki Miyata [b,c] and Takeshi Fukuma *[a,b,c]

The recent development of nanoendoscopy atomic force microscopy (NE-AFM) has enabled direct imaging of nanodynamics within living cells. However, this technique involves repeated nanoneedle tip insertions or 2D scans of the inserted tip, raising concerns about its impact on cellular viability and function. Although previous fluorometric assays indicated no lethal damage to cells, the potential effects on cellular functions remain unclear. To address this issue, we have investigated the influence of 2D/3D NE-AFM imaging on cell proliferation and calcium stress responses. Our findings reveal that typical 2D/3D NE-AFM imaging conditions do not significantly affect cell division intervals. For calcium stress responses, 2D imaging with a scan size smaller than 1 μm minimally induces calcium responses, whereas 3D imaging triggers transient calcium responses at the beginning of the scan. These responses stabilize within ~15 minutes, allowing intracellular calcium levels to return to baseline for the remaining imaging period. This study contributes to establishing conditions for NE-AFM imaging with a minimal impact on the cell functions, facilitating accurate interpretation of the obtained results, and advancing our understanding of various intracellular nanodynamics.

Received 23rd May 2025,
Accepted 28th August 2025

DOI: 10.1039/d5nr02195b

rsc.li/nanoscale

1. Introduction

Understanding nanoscale dynamics inside living cells is crucial for elucidating the fundamental mechanisms of various life phenomena such as development, aging, and diseases.[1,2] However, this has been impeded by the difficulties in directly visualizing nanodynamics in living cells. Although super-resolution fluorescence microscopy has enabled observing distributions or trajectories of labeled molecules with nanoscale precision in living cells, it does not allow imaging structural changes of target molecules themselves or unlabeled molecules.[3–5] In addition, fluorescent probes, often having a comparable size to the target molecule, can potentially alter the intracellular dynamics, especially at a nanoscale.[6] Cryo-electron microscopy is becoming increasingly powerful and is now capable of visualizing intracellular 3D nanostructures. However, it does not allow imaging nanodynamics in a living cell.[7,8] In contrast to these major bio-imaging techniques, atomic force microscopy (AFM)[9] allows direct visualization of nanoscale structural changes of individual biomolecules in a physiological solution.[10–13] However, such nanoscale imaging by conventional AFM is possible only for the biomolecules bound to a solid substrate.

To overcome this limitation, we recently developed nanoendoscopy AFM (NE-AFM). In this method, we vertically insert a needle-like tip into a live cell to perform 2D/3D AFM measurements of intra-cellular nanodynamics.[14–16] So far, 3D imaging of whole cell structures, nucleus, and actin stress fibers, and 2D imaging of dynamic structural changes of nanoscale cortical actin fiber network have been reported. Considering that this imaging technique requires inserting a long needle tip multiple times into a cell, concerns naturally arise about the cell's condition after the measurement. To examine this point, it is crucial to confirm cell viability after NE-AFM measurements.

So far, cell viability after AFM experiments has been tested by various methods. Schaus *et al.* reported non-invasiveness of amplitude modulation AFM (AM-AFM) imaging of a living cell by the fluorometric viability assay using Calcein-AM and Ethidium homodimer-1 (EthD-1).[17] Nakamura and co-workers comprehensively studied the impacts of nanoneedle insertion

[a]*Division of Nano Life Science, Kanazawa University, Kakuma-machi, Kanazawa 920-1192, Japan. E-mail: fukuma@staff.kanazawa-u.ac.jp*
[b]*Nano Life Science Institute (WPI-NanoLSI), Kanazawa University, Kakuma-machi, Kanazawa 920-1192, Japan*
[c]*Faculty of Frontier Engineering, Kanazawa University, Kakuma-machi, Kanazawa 920-1192, Japan*

into a living cell, using DAPI exclusion test, cell division test, transcriptional inhibition test, calcium response test by Fluo-4 and nuclear deformation observation.[18–22] Shibata *et al.* also reported cell viability by Calcein-AM testing after intracellular tip-enhanced Raman spectroscopy with a functionalized AFM tip inserted into a living cell.[23] Meanwhile, Schrlau *et al.* and Singhal *et al.* demonstrated lower invasiveness of a carbon nanopipette or carbon nanotube insertion than a glass pipette insertion into a living cell by monitoring calcium response using Fura-2 AM or Fluo-4 AM.[24,25] These previous studies have demonstrated that several times insertions into a living cell with a 200 nm diameter nanoneedle or nanopipette does not give a severe damage to a cell.

Compared with these AFM or nanopipette experiments, 3D NE-AFM imaging requires larger number of tip insertion with a higher frequency and density. For example, a 64 × 64 pix^2 and 40 × 40 × 8 μm^3 imaging with 20 μm s^{-1} tip velocity requires 4096 times insertions at 1.25 Hz with a 625 nm spacing. Meanwhile, 2D NE-AFM imaging, where an inserted tip is laterally scanned on an intercellular interface, may give totally different impacts on the cell viability than nanoneedle insertions. Thus, further studies are necessary to clarify these impacts on cell viability.

In our previous study, we used a fluorometric cell viability assay with Calcein-AM and propidium iodide (PI) to verify cell viability after 2D and 3D NE-AFM observations of a living cell, showing that cells remain viable for more than several hours.[15] However, this method only confirms specific functions such as esterase activity and cell membrane permeability control and does not guarantee proper functioning of other cellular functions, highlighting the need for comprehensive assessment.

In this study, we investigate the influence of 2D/3D NE-AFM measurements on cell viability by the cell division test and calcium stress response test. These two methods, except for the fluorometric assay, are more widely used than other methods such as DAPI exclusion, transcriptional inhibition, or nuclear deformation test. Besides, while most methods test only a few specific cell functions, cell division with a proper doubling time requires the proper functioning of various cellular activities, highlighting its particular importance.

2. Materials and methods

2.1 Cell culture

HeLa cells (Japanese Collection of Research Bioresources) were cultured in Dulbecco's Modified Eagle's Medium (DMEM, Fujifilm Wako Pure Chemical Corporation) supplemented with 10% fetal bovine serum (FBS, Biosera) and 1% penicillin–streptomycin (Fujifilm Wako Pure Chemical Corporation). The cells were detached by treatment with 0.05% trypsin/EDTA for 2 minutes at 37 °C and collected by centrifugation at 1400 rpm for 3 minutes. A total of 4 × 10^4 cells were then seeded into 35 mm Petri dishes (μ-Dish 35 mm low Grid-500, ibidi) and incubated in DMEM supplemented with 10% fetal bovine serum and 1% penicillin–streptomycin for 24 hours. Prior to the NE-AFM experiment, the medium was replaced with Leibovitz L-15 medium (Fujifilm Wako Pure Chemical Corporation) supplemented with 5% penicillin–streptomycin.

2.2 AFM needle tip fabrication

Two different AFM needle tips were used in NE-AFM experiments. For whole-cell 3D NE-AFM, a long tip was employed to cover the full height of the cell, while a short tip was used for 2D NE-AFM imaging inside the cell due to its easier fabrication. For long-tip fabrication, a 240AC-NG cantilever (OPUS, spring constant 2 N m^{-1}) was used, and the needle tip was fabricated using an FIB-milling method with a Helios G4 CX Dual Beam system (FEI, Thermo Fisher Scientific) as described previously.[16] This milling process was carried out at an accelerating voltage of 16 kV, a beam current of 1.3 nA, and a 4.1 mm working distance. As the tip narrowed, the ion beam current was reduced from 1.3 nA to 15 pA to avoid damage and tip apex bending. This method produced nanoneedles with lengths exceeding 10 μm, less than 200 nm base diameter, and 50 nm apex radius.

To fabricate a short needle tip, BL-AC40TS (Olympus, spring constant 0.09 N m^{-1}) cantilevers were used with the EBD method in the Helios G4 CX Dual Beam system, as described previously.[16] This process was carried out at an accelerating voltage of 15 kV and a beam current of 0.17 nA, with a working distance of 4.1 mm. With this protocol, nanoneedles with a 4 μm length and 30 nm apex radius were fabricated.

2.3 Cell division test after 2D and 3D NE-AFM

To assess the impact of AFM measurements on critical cellular functions, we conducted 3D NE-AFM and subsequently evaluated cell division. AFM measurement was performed by JPK Nanowizard IV BioAFM (Bruker Nano GmbH) combined with an inverted fluorescence microscope (Eclipse Ti2, Nikon). The cells were placed in a 37 °C preheated Petri dish heater on the stage. Measurement parameters varied depending on cell types and objectives. For 3D NE-AFM, we measured four HeLa cells (Fig. 1e(i)) using FIB-milled 240AC-NG cantilevers. Measurement parameters for the first three cells were as follows: QI mode, 5 nN force setpoint, 64 × 64 × 1000 pix^3, 15 μm s^{-1} vertical speed, and volumes of 40 × 40 × 7.5 μm^3, 35 × 35 × 7.5 μm^3, and 45 × 45 × 7.5 μm^3, respectively. The fourth cell was measured with QI mode, a 5 nN force setpoint, 64 × 64 × 800 pix^3, 20 μm s^{-1} vertical speed, and a volume of 40 × 40 × 8 μm^3.

For 2D NE-AFM, AM mode was used. Initially, an *F*–*z* curve was taken at the area of interest to identify the upper and lower cell membrane positions. An *A*–*z* curve was extracted and shown with the simultaneously obtained *F*–*z* curve in Fig. 2c. After manually adjusting the nanoneedle's *z* position at approximately 100 nm above the bottom cell membrane, the tip–sample distance feedback was turned on to allow the nanoneedle to approach the bottom cell membrane and then waited for 2 minutes to stabilize the tip position before performing 2D NE-AFM imaging.

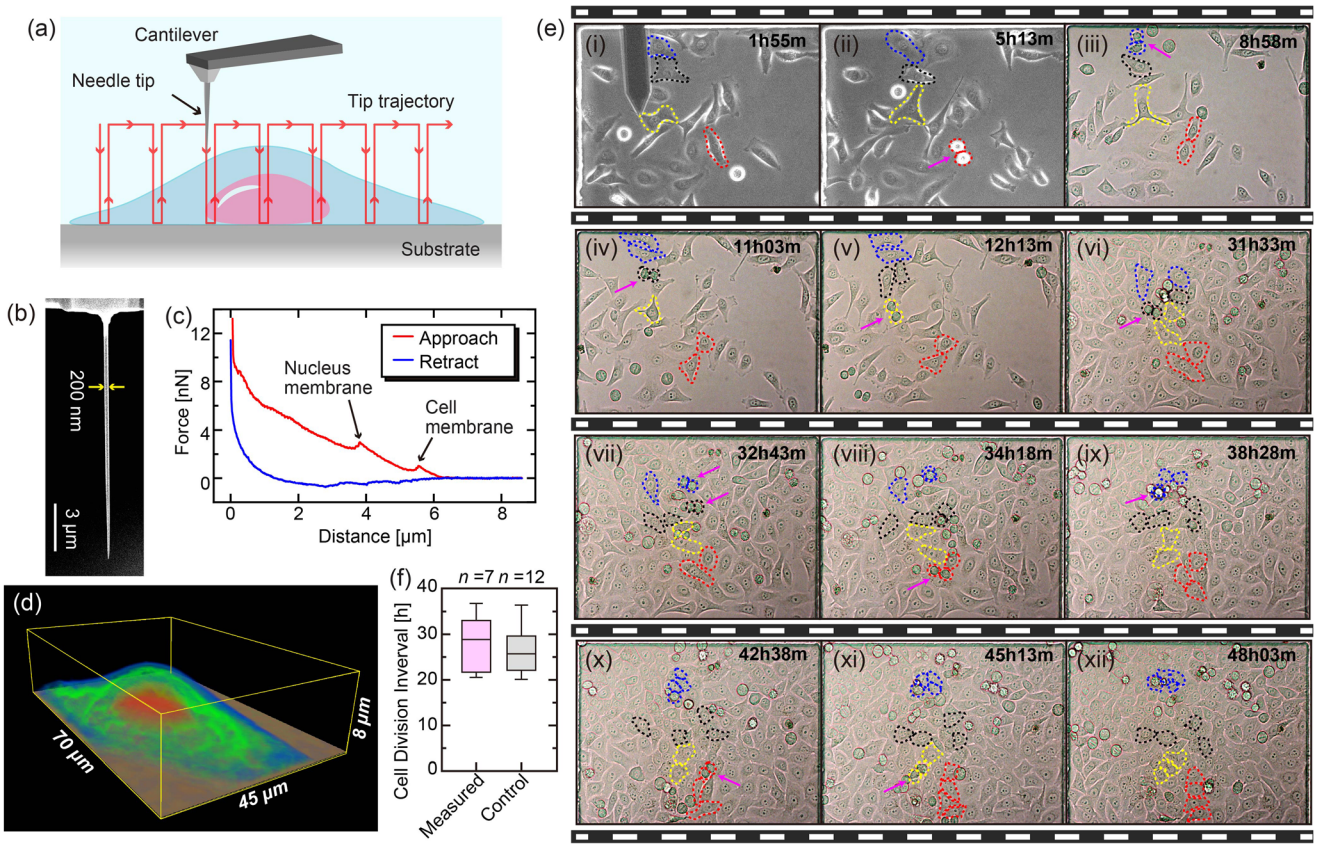

Fig. 1 (a) Schematic of the 3D NE-AFM method observing the whole cell structure. (b) FIB-fabricated nanoneedle used in the 3D NE-AFM measurements (c) typical *F*–*z* curves obtained over the nucleus area of the cell. The approach curve shows peaks corresponding to the tip penetrations of the cell and nuclear membranes. (d) Volume rendering of a 3D force map obtained by 3D NE-AFM imaging of a HeLa cel (70 × 45 × 8 μm^3). (e) Time-lapse optical micrographs of the HeLa cells, including those observed by 3D NE-AFM, highlighted with red, yellow, black, and blue dotted lines. (f) Boxplots showing distributions of cell cycle durations of the measured and control cells.

Four HeLa cells (Fig. 2f(i)) were scanned with different scan sizes up to 2 μm using a BL-AC40TS cantilever with an EBD-fabricated tip. The free oscillation amplitude was set at 20 nm, with an amplitude set point of 12 nm. The scanning size for the four cells were 0.5 × 0.5 μm^2 (red), 1 × 1 μm^2 (yellow), 1.5 × 1.5 μm^2 (black), and 2 × 2 μm^2 (blue), each captured at a resolution of 128 × 128 pix^2 with a scan rate of 1 Hz.

After the measurement, the medium was replaced with 4 mL of fresh Leibovitz L-15 medium in the Petri dish. The dish was sealed with parafilm tape and monitored with bright field imaging every 5 minutes using the perfect focus system (PFS, Nikon) on a 37 °C heated Petri dish heater for 50 hours.

2.4 Intracellular calcium imaging

One day prior to NE-AFM experiments, HeLa cells were cultured in a 35 mm glass-bottom dish in the DMEM supplemented with 10% FBS and 1% penicillin–streptomycin. The medium was replaced with Leibovitz L-15 supplemented with 5% penicillin–streptomycin and 4 μM Fluo 8-AM (ab142773, Abcam) and incubated at 37 °C for 45 minutes. Cells were then washed three times with L-15 medium, and 2 mL of Leibovitz L-15 medium was added.

Stress response experiments were performed using an Abberior Expert Line confocal microscope (Abberior Instruments) combined with a JPK Nanowizard ULTRA Speed 2 (Bruker Nano GmbH). 2D NE-AFM experiments were conducted in AM mode using a BL-AC40TS cantilever with an EBD fabricated nanoneedle tip. Time-lapse confocal images were recorded at a resolution of 450 × 450 nm^2 per pixel, in parallel with NE-AFM measurements. Imaging was performed with a 100× oil-immersion objective lens, laser excitation at 488 nm, and a GFP filter. Multiple NE-AFM measurements were performed during a single time-lapse fluorescent measurement with a scan interval long enough to allow calcium intensity to return to the baseline. After the experiments, confocal images were analyzed using ImageJ software (National Institute of Health) and Igor Pro (WaveMetrics).

To evaluate the effect of scan size, 18 cells were measured at the same location with increasing scan sizes from 0.5 μm to 3 μm with a 0.5 μm increment. 2D NE-AFM imaging was performed at a resolution of 128 × 128 pix^2 with a scan rate of 1 Hz. The influence of scan location was tested by scanning three random regions in each cell. The resolution and scan rate were the same as described above, with a total of 10 cells

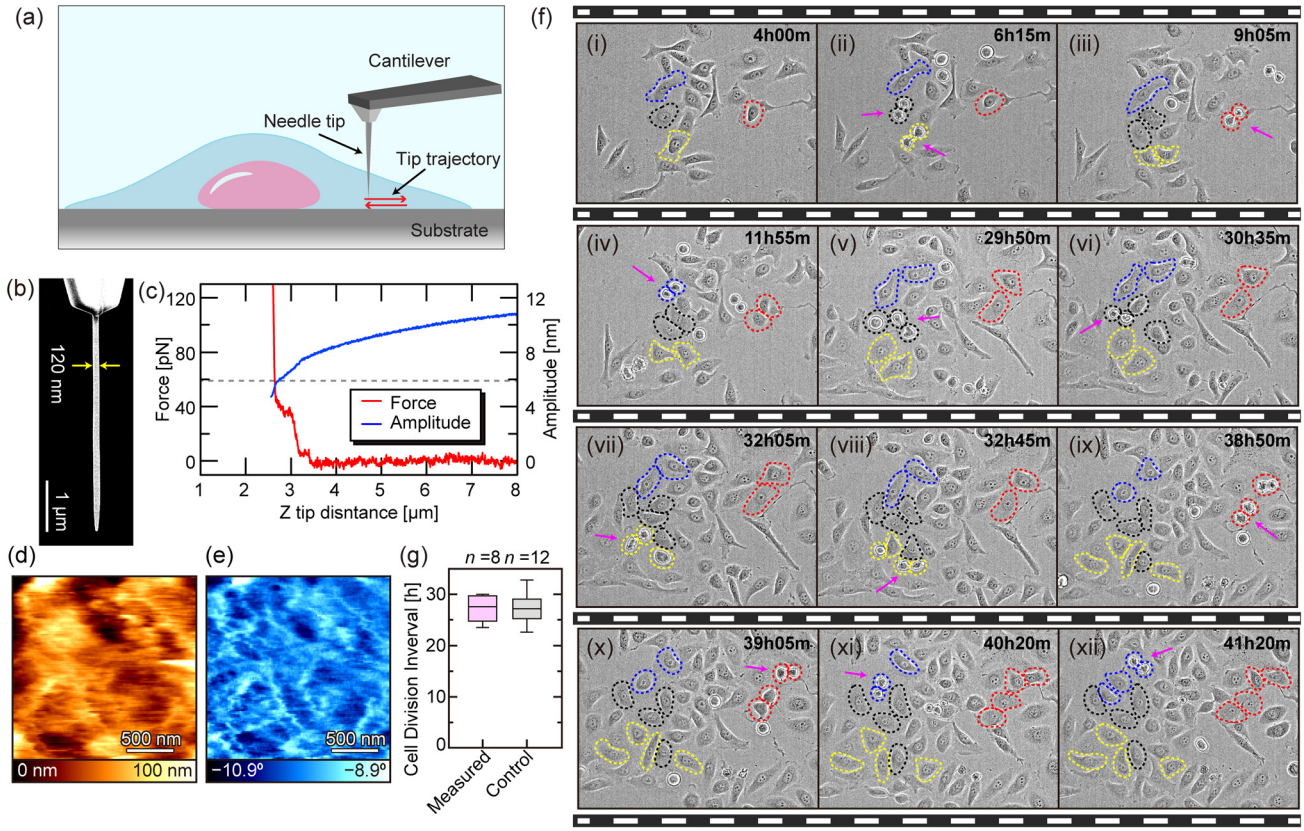

Fig. 2 (a) Schematic of the 2D NE-AFM method observing the inner surface of the bottom cell membrane. (b) EBD-fabricated nanoneedle tip used in the 2D NE-AFM measurements. (c) *F*–*z* (red) and *A*–*z* (blue) curves obtained before the 2D NE-AFM imaging to precisely identify the upper and lower cell membrane positions. (d and e) Example height (d) and phase (e) images of the inner surface of the bottom cell membrane obtained by 2D NE-AFM. (f) Time-lapse optical micrographs of the HeLa cells, including those observed by 2D NE-AFM, highlighted with red, yellow, black, and blue dotted lines. (g) Boxplots showing cell cycle duration distributions of the measured and control cells.

analyzed for each scan size (0.5 μm, 1 μm, 1.5 μm, and 2 μm). Finally, the effect of tip velocity was examined by scanning the tip at a fixed scan size of 1.5 μm with a resolution of 128 × 128 pix^2, while varying the tip velocity (1 μm s^{-1}, 3.4 μm s^{-1}, and 6 μm s^{-1}).

To investigate the influence of tip insertion on stress response, a total of 15 HeLa cells were studied using FIB-milled 240AC-NG cantilevers *via* contact-mode force spectroscopy. Each cell underwent sequential insertions at five times on the cell periphery, followed by five insertions on the nucleus, with the tip moving at a speed of 20 μm s^{-1} and intervals of 30 seconds between insertions (Fig. 4a–e). Subsequently, comprehensive 3D NE-AFM imaging and simultaneous time-lapse fluorescence measurements were conducted following the method described above. 3D NE-AFM imaging was conducted in the QI mode with force setpoint of 8 nN, resolution of 64 × 64 × 1000 pix^3, vertical tip scan speed of 20 μm s^{-1}, and scanned volume of 64 × 41 × 8 μm^3.

2.5 Statistical methods

All statistical calculations were performed using GraphPad Prism 9 and Microsoft Excel.

3. Results and discussion

To understand the effect of 3D NE-AFM on cell proliferation, we have performed 3D measurements of the whole cell, as shown in Fig. 1. The operation principle of 3D NE-AFM is presented in Fig. 1a. A needle tip is repeatedly inserted in the cell through a selected area to achieve force *versus* distance (*F*–*z*) curves. The tip length should be sufficient to reach the substrate after penetrating the cell membrane. Previous reports and our experience consistently suggest that sharp tip apex and tip diameter should not exceed 200 nm for non-invasive tip insertion.[14,26–28] A tip with 12 μm length and 200 nm base diameter was used in this experiment as shown in Fig. 1b. This needle tip was fabricated by milling a tetrahedral tip, which comes with a commercial Si cantilever (240AC-NG, OPUS, spring constant: k = 2 N m^{-1}), by focused ion beam (FIB).[16] A typical *F*–*z* curve obtained on the cell nucleus, where the cell has the maximum height, is represented in Fig. 1c. When the tip approaches the cell, the cantilever initially detects no forces. As the tip comes in contact with the cell surface, the force exerted on the tip increases and the cantilever starts to bend gradually until the force is enough to penetrate the cell membrane. As the tip penetrates the upper cell

membrane, the force decreases, resulting in a sharp peak in the *F*–*z* curve. Then, the tip continues to go down and reach the nucleus membrane, where the force again starts to increase until it becomes enough to penetrate the nucleus membrane. As a result, another sharp peak introduced in the *F*–*z* curve indicates nucleus membrane penetration. The tip approach was continued through the cell nucleus until the force abruptly increased, which indicates that the tip reached the substrate. Then, the tip starts retracting to get out of the cell, producing a retract curve (blue line in Fig. 1c). By taking *F*–*z* curves at arrayed-*xy* positions, we can obtain a 3D force map representing the distribution of intracellular components. An example 3D NE-AFM image of a whole cell is presented in Fig. 1d, where the nucleus can be distinguished from other parts of the cell.

We performed 3D NE-AFM measurements of four different HeLa cells and then monitored them until their next division. The four measured cells are highlighted with red, yellow, black, and blue dotted lines in Fig. 1e(i). After 5 hours since we started the NE-AFM imaging, the first measured cell (red) was divided (Fig. 1e(ii)), and then the fourth (blue), third (black), and second (yellow) measured cells were divided respectively in Fig. 1e(iii–v). After confirming all the measured cell divisions, we tracked all the daughter cells until the next division to determine the complete cell cycle duration. After 45 hours, most of the daughter cells' division was also confirmed, as shown in Fig. 1e(vi–xii). Only one daughter cell from the second measured cell remained undivided. Several reasons might explain why the daughter cells followed different fates, with one continuing to divide while another remained undivided. Examples include asymmetric cell division, local microenvironmental influences, distinct gene expression profiles, cell–cell communication, and specific signaling molecules.[29–36] Meanwhile, the observed cell death does not necessarily suggest the invasiveness of the NE-AFM measurement. We observed 4 times and then 8 times divisions from the 4 parent cells. Out of 12 times divisions, it failed only once. On the other hand, the failure ratio in 72 times divisions of control cells (*i.e.*, cells without NE-AFM measurements) was found to be once in every 9 divisions, which is higher than that for the observed cells.

We compared the cell cycle duration of measured daughter cells and control cells. HeLa cells typically divide in 24 hours, but this can vary by several hours depending on the cell line sources, experimental environments, measurement conditions, *etc*.[37–40] In this study, both measured and control cells showed the cell cycle duration within this range. In Fig. 1f, the boxplots show that the difference in the cell cycle durations between the measured and control cells is not significant. Control cells took ~25 hours to complete a cell cycle, while the measured cells took ~27 hours. These results suggest that this type of measurement does not perturb cell cycle progression. Various cellular functions are involved in the cell division process, and this result assures that 3D NE-AFM does not significantly affect those functionalities.

The cell maintains normal viability after 3D NE-AFM, which suggests that the tip apex can be safely positioned anywhere inside a living cell to perform a local 2D/3D NE-AFM measurement. Particularly at the intracellular interfaces, we can take advantage of the high-resolution imaging capability of 2D NE-AFM. Here, we investigate the invasiveness of such measurements, as shown in Fig. 2.

The principle of 2D NE-AFM is illustrated in Fig. 2a. A needle tip is inserted and placed on the lower cell membrane in the periphery area. A needle tip with a base diameter of ~120 nm, an apex radius of ~30 nm, and a length of 4 μm was used, as shown in Fig. 2b. The needle tips were fabricated on a commercially available cantilever (BL-AC40TS-C2, OLYMPUS, spring constant: $k = 0.09$ N m^{-1}) using the electron beam deposition (EBD) technique.[16] For 2D NE-AFM imaging, we used amplitude modulation (AM) mode, where the cantilever oscillation amplitude was detected for the tip–sample distance regulation. Then, the needle tip was placed above the cell periphery area to achieve an *F*–*z* curve (red) and an amplitude *versus* distance (*A*–*z*) curve (blue), as shown in Fig. 2c. Initially, the vertical force is zero and starts to increase when the tip comes in contact with the upper cell membrane. Afterward, the force increases gradually and then sharply increases when the tip reaches the bottom cell membrane supported by the substrate. Once the location of the bottom cell membrane was determined from the *F*–*z* curve, we chose a feedback setpoint (dotted gray line in Fig. 2c) from its relevant *A*–*z* curve. After the nanoneedle was properly positioned over the target area, it was inserted into a cell 100 nm above the bottom membrane by manually adjusting the *Z* tip position. Then, the tip–sample distance feedback was turned on to allow the nanoneedle to reach the bottom cell membrane and we waited 2 minutes to stabilize the tip position before performing a 2D NE-AFM imaging.

In this experiment, 2 × 2 μm^2 height and phase images were obtained simultaneously, as shown in Fig. 2d and e, where we see fibrillar features on the bottom cell membrane. Similar to the experiments for 3D NE-AFM (Fig. 1), we performed cell division tests after such 2D NE-AFM observation. In the case of 2D NE-AFM, the scanning area is crucial because of the lateral movements of the tip inside a living cell. A previous study confirmed that local 2D NE-AFM imaging with a scanning area smaller than 2 × 2 μm^2 hardly influences cell viability.[15] Here, we performed 2D NE-AFM measurements of four different HeLa cells with different scanning areas and then monitored them until their next division. The four measured cells with different scanning areas are highlighted with red (0.5 × 0.5 μm^2), yellow (1 × 1 μm^2), black (1.5 × 1.5 μm^2), and blue (2 × 2 μm^2) dotted lines in Fig. 2f(i). After 6 hours since we started the NE-AFM imaging, the second (yellow) and third (black) measured cells were divided (Fig. 2f (ii)), and then the first (red), and fourth (blue) measured cells were divided, respectively in Fig. 2f(iii) and (iv). After confirming all the measured-cell divisions, we observed all the daughter cells until the next division to determine the complete cell cycle durations. After 41 hours, most of the daughter cells' divisions were confirmed as shown in Fig. 2f(v-xii). In this experiment, all daughter cells were divided within a reasonable dur-

ation for both measured and control cells as shown in Fig. 2g. No significant difference was observed between them. These results suggest that with a scanning area smaller than 2 × 2 μm^2, 2D NE-AFM does not significantly affect cell cycle progression. To validate the reproducibility and improve the statistical reliability of the results, additional NE-AFM measurements were performed under the same experimental conditions. The outcomes, summarized in Fig. S1, confirm consistent division intervals between control and measured groups, with no statistically significant differences observed.

We investigated the calcium stress response of the cells caused by 2D NE-AFM by monitoring the calcium concentration changes. To this end, we stained the cells with Fluo-8 AM, an intracellular calcium ion indicator, and monitored its fluorescence intensity by confocal microscopy during 2D NE-AFM imaging of an inner surface of the bottom cell membrane. In 2D NE-AFM imaging, a cell may get mechanical stress depending on the scan size, scan locations, or tip velocity. In this experiment, we investigate the dependency on these three parameters.

First, we test stress response dependency on the scan size. We performed 2D NE-AFM at the same place with six different scan sizes from 0.5 × 0.5 μm^2 to 3 × 3 μm^2. An example optical image of the measured cell is illustrated in Fig. 3a. The red square indicates the scanned area. During the scan, we monitored the fluorescence intensity changes as illustrated in Fig. 3b. We waited a few minutes at the beginning and between each AFM measurement to get the stable fluorescence intensity as indicated by the black lines in Fig. 3b. First, we applied 0.5 × 0.5 μm^2 scan size and observed the calcium intensity response during AFM measurement. Then, we waited a few minutes to ensure that the fluorescence intensity was stabilized and moved to the next scan size. In this experiment, there were no significant changes in the intracellular calcium concentration for 0.5 μm (red), 1 μm (navy blue), and 1.5 μm (green) scan sizes, whereas a strong increase in intracellular calcium concentration was observed for 2 μm (magenta), 2.5 μm (orange), and 3 μm (light blue) scan sizes (Fig. 3b). Fig. 3c and d respectively show fluorescence microscopy images obtained at t_1 and t_2 indicated in Fig. 3b. The former image indicates no stress response, while the latter shows a strong stress response. We repeated this experiment 18 times, and the results are summarized in a bar chart showing the calcium response probability for each scan size in Fig. 3e. While the probability is negligibly small for a scan size less than 1 μm, it significantly increases when the scan size exceeds 1 μm.

We also investigated whether the location of the scan on the cell influences the likelihood of inducing a response. Fig. 3f shows an example of three locations (red boxes) selected for the 2D NE-AFM imaging. In this way, we selected three locations within each of the ten cells for each scan size (0.5 μm, 1 μm, 1.5 μm, and 2 μm), as shown in Fig. 3g. For the smaller scan sizes (0.5 μm and 1 μm), most cells showed no response at any of the three locations. On the other hand, for larger scan sizes (1.5 μm and 2 μm), most of the cells showed

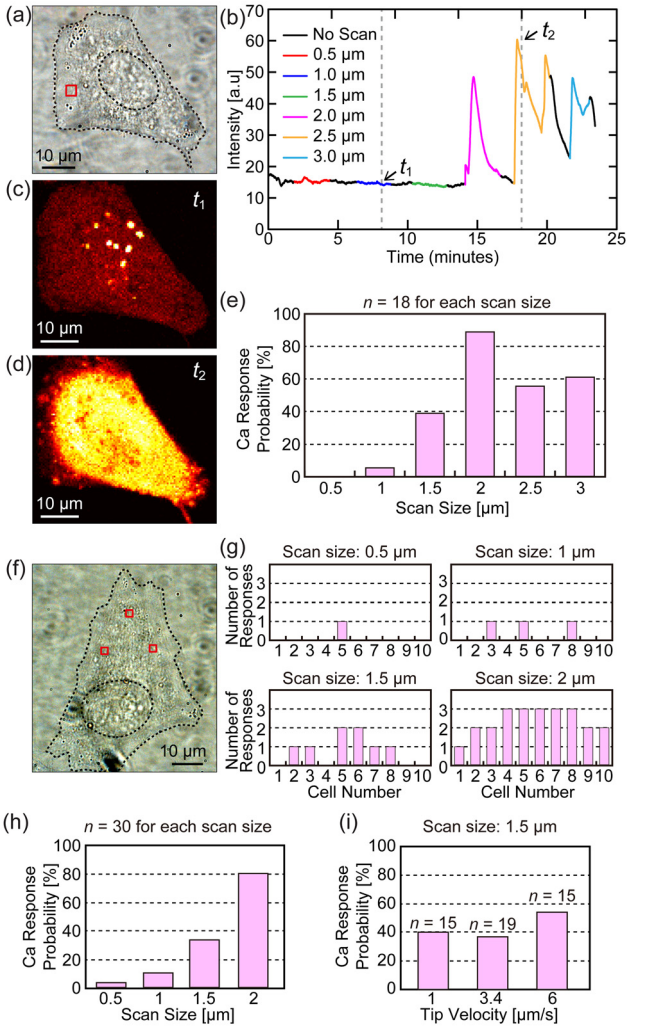

Fig. 3 Calcium response tests of the cells imaged by 2D NE-AFM. (a) Example optical image of the measured cell, with the red square indicating the scanned area. (b) Time-lapse changes in the fluorescence intensity during the multiple 2D NE-AFM observations with different scan sizes. The black lines indicate waiting periods between observations. (c and d) Fluorescence micrographs taken at time points t_1 (c) and t_2 (d). (e) Calcium response probability for each scan size. (f) Example optical image of the measured cell, showing three selected locations (red boxes) used for 2D NE-AFM imaging to assess the effect of scan location on the stress response. (g) Number of Calcium responses at the three selected locations across ten cells for each scan size (0.5 μm, 1 μm, 1.5 μm, and 2 μm). (h) Calcium response probability for each scan size estimated from all data shown in (g). (i) Calcium response probabilities for three different tip velocities (1 μm s^{-1}, 3.4 μm s^{-1}, and 6 μm s^{-1}) with a scan size of 1.5 μm.

responses at two or all three locations. All these results are summarized in the probability chart in Fig. 3h, demonstrating the high probability over 1 μm scan. This is consistent with the results shown in Fig. 3e. This suggests that the probability of calcium response does not depend on location but on scan size.

We also test the calcium response dependency on tip velocity. With 1.5 μm scan size, we apply different tip velocities

separately for n cells, where n denotes the number of measured cells. Fig. 3i represents the calcium response probabilities measured with three different tip velocities (1 μm s^{-1}, 3.4 μm s^{-1}, and 6 μm s^{-1}). Although 6 μm s^{-1} provided a higher response probability than the other speeds, the 3.4 μm s^{-1} showed a lower probability than 1 μm s^{-1}. Overall, the tip velocity dependence is not so evident within the tested speed range (*i.e.*, <6 μm s^{-1}), where we can stably perform 2D NE-AFM with the present AFM system.

These findings suggest that scan size is the dominant factor influencing the calcium response, while scan location and tip velocity appear to have a minimal effect. Therefore, 2D NE-AFM imaging with a scan size of less than 1 μm can be safely used for intracellular investigation without causing severe damage or stress to a cell.

Here, we consider the results' implications based on the mechanisms of calcium response. According to previous reports, mechanosensitive (MS) channels on a cell surface open when cells feel mechanical stress, inducing a small amount of calcium influx. This calcium increase further induces calcium release from the endoplasmic reticulum (ER) leading to a significant and rapid calcium increase in a cell.[41–43] Another possibility is that, because there are also MS channels on the ER,[41] the cantilever tip can directly stimulate these channels and cause an increase in Ca in the cytoplasm. In our experiments, the lateral tip scan may induce a calcium influx in two ways: giving mechanical stress to MS channels or creating a leakage path at the tip-membrane interface. A larger scan should disturb more intracellular organizations, increasing the chance of giving stress to MS channels. Meanwhile, a faster scan should increase the risk of leakage at the tip-membrane interface, while the disturbed components should not increase significantly. Therefore, the strong scan-size dependence and weak tip-velocity dependence suggest that the calcium response is mainly caused by the opening of MS channels due to the tip-induced mechanical stress for a scan speed of less than 6 μm s^{-1}.

During 3D NE-AFM imaging, a nanoneedle tip is repeatedly inserted into a cell. Thus, we first investigated the calcium response induced by the tip insertions. We performed up to five consecutive insertions at a fixed position of the cell periphery or nucleus region with 30 second intervals and monitored the subsequent calcium fluorescent intensity changes. Fig. 4a presents a representative optical image of a measured cell, where red squares denote the insertion sites. Similar experiments were performed on 15 cells, and the number of insertions required to elicit a calcium response was summarized in Fig. 4b and c. Note that "NA" indicates the cases where no response was observed. Comparing these distributions, we found that cells are more sensitive to the insertions on a nucleus than at their periphery. At the periphery, eight out of 15 cells showed no response, as illustrated in Fig. 4d. In contrast, on the nucleus, eight out of 15 cells showed a calcium response to the first or second tip insertion, as illustrated in Fig. 4e.

This difference may be explained by the difference in the cell membrane area deformed by the tip insertion. A nucleus is typically located at the center of a cell and the cell membrane above nucleus is relatively high. Thus, the tip insertion on a nucleus likely deforms a larger cell membrane area for a longer time than that at the periphery, leading to a higher chance to give mechanical stress to the MS channels on cell membrane. Meanwhile, even at the cell periphery, seven out of 15 cells showed a calcium response.

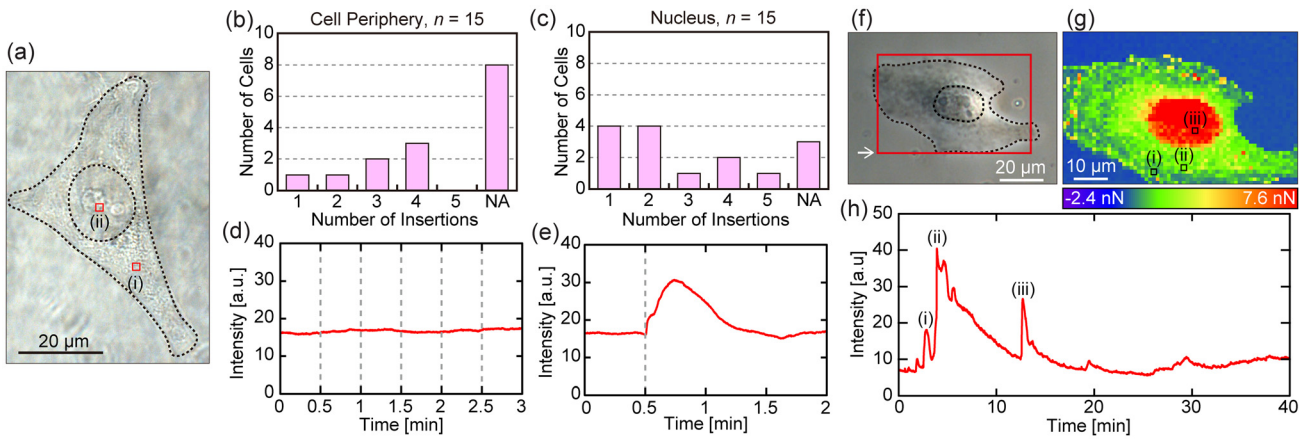

Fig. 4 Calcium response tests upon repeated nanoneedle insertions or 3D NE-AFM. (a) A representative optical image of a measured cell, with red squares indicating the nanoneedle insertion sites on the (i) periphery and (ii) nucleus. (b and c) Distributions of the number of insertions required for inducing Calcium response on the (b) cell periphery and (c) nucleus (n = 15 cells). Each cell underwent up to five consecutive penetrations at 30 second intervals, with the procedure stopped when a Calcium response was observed. "NA" indicates cells that did not respond to any of the five. (d and e) Fluorescence intensity changes during nanoneedle insertions performed with 30 second intervals (dotted lines). (d) An example showing no response after five insertions at cell periphery. (e) An example showing response after the first insertions on cell nucleus. (f) Example optical image of a cell measured by 3D NE-AFM, with a red square indicating the scanned area and a white arrow showing the scanning start point and direction. (g) *XY* cross-sectional image obtained from the 3D force map near the substrate height. (h) Fluorescence intensity changes during 3D NE-AFM imaging. The peaks (i)–(iii) were observed at the positions indicated in (g).

Thus, it is unlikely that we can avoid such calcium increases for a 3D NE-AFM imaging where thousands of tip insertions are required.

To confirm this expectation, we performed 3D NE-AFM imaging of the whole cell structure and monitored calcium fluorescence intensity changes during the imaging. Fig. 4f shows an example optical image of a cell measured by 3D NE-AFM, with a red square indicating the scanned area and the white arrow showing the start position and direction of the tip scan. Fig. 4g shows an *XY* cross section of the 3D force map taken near the substrate height. Fig. 4h shows calcium fluorescence intensity changes during the 3D NE-AFM imaging. This profile shows three strong peaks (i)–(iii) at the beginning of the 3D scan, but no prominent peaks afterward. This behavior does not depend on tip velocity, scan size, or tip location and is observed even with a small scan size at a cell periphery. These results confirm our expectation that it is almost impossible to perform 3D NE-AFM without inducing a calcium response.

As indicated in Fig. 4g, peaks (i) and (ii) were observed at the cell periphery while peak (iii) was observed on the nucleus. Thus, the peaks are not necessarily observed on the nucleus but also at the cell periphery, which is consistent with our tip insertion experiments explained above. After these initial responses for ~15 minutes, the cell became insensitive to the repeated tip insertions. This behavior is consistent with the previous studies reporting that MS channels become insensitive when they are subject to sustained mechanical stress.[44,45] Therefore, when we interpret the results obtained by 3D NE-AFM, we should carefully take into account the initial calcium increase. However, as the calcium concentration returns to the normal value in ~15 minutes, such an impact is not significant in the rest of the imaging time. The transient calcium response likely reflects mechanosensitive channel desensitization, serving to protect cells from prolonged calcium overload and its potential dysfunction. Previous studies have shown that calcium responses induced by nanoscale insertions are transient and not associated with loss of viability or membrane integrity.[24,25] Consistent with these findings, we observed that calcium levels returned to baseline shortly after NE-AFM imaging, and no delay in cell division was noted, while long-term consequences of such brief calcium events remain to be fully explored.

4. Conclusions

In this study, we have investigated the influence of 2D/3D NE-AFM measurements on cell proliferation and calcium stress response. No significant difference in the cell cycle duration was found between the measured and control cells after 2D/3D NE-AFM measurements (Fig. 1 and 2). These results ensure that, under appropriate conditions, NE-AFM techniques are safe for intracellular investigation without causing fatal damage. The calcium response test during 2D NE-AFM measurements revealed that scanning an area smaller than 1 μm does not trigger a significant calcium response, suggesting that the mechanical stress from the AFM tip scan is minimal under appropriate conditions. Moreover, tip velocity (<6 μm s^{-1}) and location have no major effect on inducing calcium response. All these results suggest that NE-AFM can investigate intercellular properties without causing significant harm to cell proliferation or calcium balance. However, we found that cells show strong stress responses at the beginning of a 3D NE-AFM imaging, which should be carefully considered in interpreting the results obtained by this method. These findings provide important guidelines for applying 2D/3D NE-AFM to the investigations of various intra-cellular phenomena.

This study focused on cell division and calcium response as key indicators of NE-AFM's cellular impact. However, we appreciate that further analyses, such as transcriptomics, apoptosis, and DNA damage assays would provide more profound insight in the future. In addition, we focused on HeLa cells primarily because they are one of the most widely used and well-characterized model cell lines in cell biology. Nevertheless, we also appreciate that they are relatively robust and resilient to external stimulus. Therefore, the general applicability of the findings should be further tested with more sensitive cells such as neurons or non-cancerous cells in the future.

Author contributions

T. F. conceived the study idea, designed the overall framework, coordinated activities and timelines across contributors, and secured financial support for the project. T. F. provided and maintained equipment used in this study with the support of K. Miyazawa. T. F. and M. M. H. developed and optimized the experimental protocols, curated raw datasets and structured them for publication, created figures and visual representations of the data, and drafted the initial manuscript. K. Miyata and K. Miyazawa developed custom software for data processing and analysis under the supervision of T. F. M. M. H. conducted the experiments and acquired primary data under the supervision of T. F., T. I. and K. Miyazawa. T. F., M. M. H. and T. I. performed statistical analyses and interpretation of results. All authors contributed to manuscript revision and final approval.

Conflicts of interest

The authors declare no conflict of interest.

Data availability

Data for this article are available at GitHub at **https://github.com/fukuma-lab/cell-proliferation-paper**.

Supplementary information: Fig. 1–4 and Fig. S1. See DOI: **https://doi.org/10.1039/d5nr02195b**.

Acknowledgements

This work was supported by the World Premier International Research Initiative (WPI), Ministry of Education, Culture, Sports, Science and Technology (MEXT), Japan, and the Japan Society for the Promotion of Science (JSPS) KAKENHI Grant Numbers 21H05251 and 20H00345.

References

1 A. R. Sun, R. M. Hengst and J. L. Young, *Curr. Opin. Cell Biol.*, 2024, **87**, 102322.
2 S. Suresh, *Acta Biomater.*, 2007, **3**, 413–438.
3 S. Liu, P. Hoess and J. Ries, *Annu. Rev. Biophys.*, 2022, **51**, 301–326.
4 Y. M. Sigal, R. Zhou and X. Zhuang, *Science*, 2018, **361**, 880–887.
5 L. von Diezmann, Y. Shechtman and W. E. Moerner, *Chem. Rev.*, 2017, **117**, 7244–7275.
6 K. Thorn, *Mol. Biol. Cell*, 2017, **28**, 848–857.
7 J. Frank, *J. Struct. Biol.*, 2017, **200**, 303–306.
8 V. Lučić, A. Rigort and W. Baumeister, *J. Cell Biol.*, 2013, **202**, 407–419.
9 G. Binnig, C. F. Quate and C. Gerber, *Phys. Rev. Lett.*, 1986, **56**, 930–933.
10 T. Ando, T. Uchihashi and S. Scheuring, *Chem. Rev.*, 2014, **114**, 3120–3188.
11 N. Kodera, D. Yamamoto, R. Ishikawa and T. Ando, *Nature*, 2010, **468**, 72–76.
12 Y. F. Dufrêne, T. Ando, R. Garcia, D. Alsteens, D. Martinez-Martin, A. Engel, C. Gerber and D. J. Müller, *Nat. Nanotechnol.*, 2017, **12**, 295–307.
13 C. R. Guerrero, P. D. Garcia and R. Garcia, *ACS Nano*, 2019, **13**, 9629–9637.
14 M. Penedo, T. Shirokawa, M. S. Alam, K. Miyazawa, T. Ichikawa, N. Okano, H. Furusho, C. Nakamura and T. Fukuma, *Sci. Rep.*, 2021, **11**, 7756.
15 M. Penedo, K. Miyazawa, N. Okano, H. Furusho, T. Ichikawa, M. S. Alam, K. Miyata, C. Nakamura and T. Fukuma, *Sci. Adv.*, 2021, **7**, eabj4990.
16 T. Ichikawa, M. S. Alam, M. Penedo, K. Matsumoto, S. Fujita, K. Miyazawa, H. Furusho, K. Miyata, C. Nakamura and T. Fukuma, *STAR Protoc.*, 2023, **4**, 102468.
17 S. S. Schaus and E. R. Henderson, *Biophys. J.*, 1997, **73**, 1205–1214.
18 C. Nakamura, H. Kamiishi, N. Nakamura and J. Miyake, *Electrochemistry*, 2008, **76**, 586–589.
19 S. Han, S. Ryu, T. Kitagawa, H. Uetsuka, N. Fujimori, Y. Aoki, R. Ota, C. Nakamura and J. Miyake, *Arch. Histol. Cytol.*, 2009, **72**, 261–270.
20 S. Han, C. Nakamura, I. Obataya, N. Nakamura and J. Miyake, *Biochem. Biophys. Res. Commun.*, 2005, **332**, 633–639.
21 S. Ryu, R. Kawamura, R. Naka, Y. R. Silberberg, N. Nakamura and C. Nakamura, *J. Biosci. Bioeng.*, 2013, **116**, 391–396.
22 S. Mieda, Y. Amemiya, T. Kihara, N. Nakamura, J. Miyake, C. Nakamura and K. Ishihara, *Biosens. Bioelectron.*, 2012, **31**, 323–329.
23 T. Shibata, H. Furukawa, Y. Ito, M. Nagahama, T. Hayashi, M. Ishii-Teshima and M. Nagai, *Micromachines*, 2020, **11**, 495.
24 M. G. Schrlau, E. Brailoiu, S. Patel, Y. Gogotsi, N. J. Dun and H. H. Bau, *Nanotechnology*, 2008, **19**, 325102.
25 R. Singhal, Z. Orynbayeva, R. V. K. Sundaram, J. J. Niu, S. Bhattacharyya, E. A. Vitol, M. G. Schrlau, E. S. Papazoglou, G. Friedman and Y. Gogotsi, *Nat. Nanotechnol.*, 2011, **6**, 57–64.
26 M. S. Alam, M. Penedo, T. Ichikawa, M. M. Hosain, K. Matsumoto, K. Miyazawa and T. Fukuma, *Nanoscale*, 2025, **17**, 7342–7350.
27 I. Obataya, C. Nakamura, S. Han, N. Nakamura and J. Miyake, *Biosens. Bioelectron.*, 2005, **20**, 1652–1655.
28 I. Obataya, C. Nakamura, S. Han, N. Nakamura and J. Miyake, *Nano Lett.*, 2005, **5**, 27–30.
29 J. H. Buss, K. R. Begnini and G. Lenz, *J. Cell Sci.*, 2024, **137**, jcs261400.
30 J. Nunes and D. Loeffler, *Front. Hematol.*, 2024, **3**, 1373554.
31 D. Zheng, Y. Mao, Y. Gao, F. He and J. Ma, *iScience*, 2023, **26**, 107198.
32 S. L. Spencer, S. D. Cappell, F. C. Tsai, K. W. Overton, C. L. Wang and T. Meyer, *Cell*, 2013, **155**, 369–383.
33 M. Arora, J. Moser, H. Phadke, A. A. Basha and S. L. Spencer, *Cell Rep.*, 2017, **19**, 1351–1364.
34 Z. Dong, N. Yang, S. Y. Yeo, A. Chitnis and S. Guo, *Neuron*, 2012, **74**, 65–78.
35 S. R. Pine, B. M. Ryan, L. Varticovski, A. I. Robles and C. C. Harris, *Proc. Natl. Acad. Sci. U. S. A.*, 2010, **107**, 2195–2200.
36 U. Berge, D. Bochenek, R. Schnabel, A. Wehling, T. Schroeder, T. Stadler and R. Kroschewski, *Nat. Commun.*, 2019, **10**, 1901.
37 F. M. Boisvert, Y. Ahmad, M. Gierliński, F. Charrière, D. Lamont, M. Scott, G. Barton and A. I. Lamond, *Mol. Cell. Proteomics*, 2012, **11**, M111.011429.
38 Y. Liu, Y. Mi, T. Mueller, S. Kreibich, E. G. Williams, A. Van Drogen, C. Borel, M. Frank, P.-L. Germain, I. Bludau, *et al.*, *Nat. Biotechnol.*, 2019, **37**, 314–322.
39 Y. Kumei, T. Nakajima, A. Sato, N. Kamata and S. Enomoto, *J. Cell Sci.*, 1989, **93**, 221–226.
40 S. Sato, A. Rancourt, Y. Sato and M. S. Sato, *Sci. Rep.*, 2016, **6**, 23328.
41 T. J. Kim, C. Joo, J. Seong, R. Vafabakhsh, E. L. Botvinick, M. W. Berns and A. E. Palmer, *eLife*, 2015, **4**, e04876.
42 Y. Wang, J. Shi and X. Tong, *Int. J. Mol. Sci.*, 2021, **22**, 8782.
43 M. D. R. Cantero and H. F. Cantiello, *Gene*, 2022, **827**, 146313.
44 R. Peyronnet, D. Tran, T. Girault and J.-M. Frachisse, *Front. Plant Sci.*, 2014, **5**, 558.
45 J. Hao and P. Delmas, *J. Neurosci.*, 2010, **30**, 13384–13395.